Fabrication of Highly Flexible, Scalable, and High-Performance Supercapacitors Using Polyaniline/Reduced Graphene Oxide Film with Enhanced Electrical Conductivity and Crystallinity

*Minkyu Kim, Choonghyeon Lee, and Jyongsik Jang**

With developments in technology, tremendous effort has been devoted to produce flexible, scalable, and high-performance supercapacitor electrode materials. This report presents a novel fabrication method of highly flexible and scalable electrode material for high-performance supercapacitors using solution-processed polyaniline (PANI)/reduced graphene oxide (RGO) hybrid film. SEM, TEM, Raman, and XPS analyses show that the PANI/RGO film is successfully synthesized. The percentages of the PANI component in the film are controlled (88, 76, and 60%), and the maximum electrical conductivity (906 S cm^{-1}) is observed at the PANI percentage of 76%. Notably, electrical conductivity of the PANI/RGO film (906 S cm^{-1}) is larger than both PANI (580 S cm^{-1}) and RGO (46.5 S cm^{-1}) components. XRD analysis demonstrates that the strong π–π interaction between the RGO and the PANI cause more compact packing of the PANI chains by inducing more fully expanded conformation of the PANI chains in the solution, leading to increase in the electrical conductivity and crystallinity of the film. The PANI/RGO film also displays diverse advantages as a scalable and flexible electrode material (e.g., controllable size and great flexibility). During the electrochemical tests, the film exhibits high capacitance of 431 F g^{-1} with enhanced cycling stability.

1. Introduction

With advances in technology, the various types of portable electronic equipment (e.g., electronic paper, roll-up displays, and pacemakers) are becoming more ultra-functional, and they are designed to be lightweight and flexible with controllable size.[1] However, the research on the energy-storage devices required to fulfill the criteria above is still insufficient.[1c] Accordingly, producing innovative energy-storage devices with high flexibility (function well under bending, folding, and twisting conditions), lightweight (possess more energy with less weight), and facile control in size remains a challenge.[1c,2]

M. Kim, C. Lee, Prof. J. Jang
World Class University program of Chemical Convergence for Energy & Environment
School of Chemical and Biological Engineering
Seoul National University
Seoul, 151–742, Korea
E-mail: jsjang@plaza.snu.ac.kr

DOI: 10.1002/adfm.201303282

Recently, significant effort has been devoted to realize these goals. For instance, various transition metal oxides have been incorporated with conducting polymers (CPs) as flexible electrodes for supercapacitors.[1e,3] However, electrodes consisting of transition metal oxides and CPs tend to be easily deformed under even small tensile strain, and the intrinsically low conductivity of transition metal oxides often hinders high-performance supercapacitor electrodes.[3a,4] Additionally, CPs in combination with diverse carbon materials (e.g., carbon nanofibers, and carbon nanotubes) have also been proposed as electrodes for flexible supercapacitors, and very recently, graphene and CPs composite emerged as a way to achieve the above goals.[1c,5] However, fabricated nano/micro structured carbon-CPs electrodes are usually made from pressing of powder onto electrode substrate or filtering of as-prepared solution and subsequent transfer on substrate. Therefore, fabrication of flexible supercapacitor electrodes with various sizes is limited.

Our inspiration for overcoming these limitations came from the following ideas: solution-processed CPs (such as PANI/camphorsulfonic acid (CSA),[6] PANI/Poly(4-styrenesulfonate),[7] and poly(3,4-ethylenedioxythiophene)/poly(styrenesulfonate)[8] have been extensively studied as electrode materials because they offer an easy and low-cost method of processing highly electrically conductive, flexible, and various sized thin-film electrodes with diverse substrate size. Among the various solution-processed CPs, PANI/CSA has attracted great attention as an electrode material for various energy devices due to its high electrical conductivity and excellent processability with organic solvents.[6c,e,9] Solution-processed PANI/CSA film exhibits electrical conductivity two or three orders of magnitude higher than that of pristine nanostructured PANI powder, as the film possesses a changed polymer chain conformation.[6d,10] With the help of the pertinent solvent, the compact coil conformation of the PANI chains becomes a more expanded coil conformation.[6d] The more expanded coil structure of the individual PANI chains acts to promote compact packing between polymer chains, leading

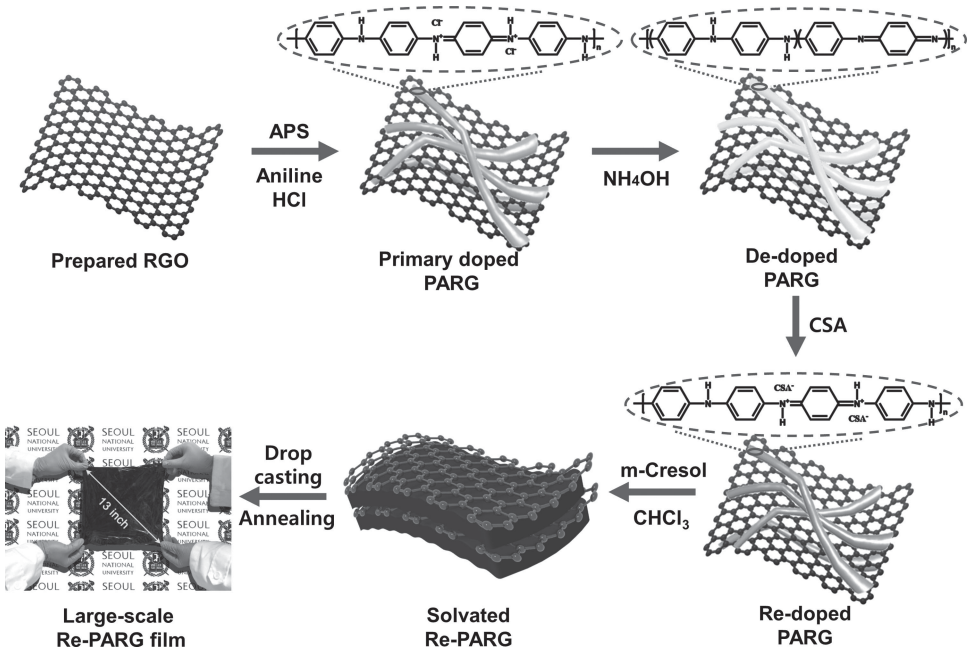

Figure 1. Schematic illustration of the sequential steps for fabricating large-scale Re-PARG film.

to increase in the electrical conductivity of the polymer with improved inter-molecular interaction and crystallinity.[6d] As stated above, molecular conformation is a crucial factor influencing the electrical conductivity as well as the overall crystalline structure of CPs. Several researchers have reported that between the quinoid ring of PANI and the basal plane of the carbon surface, a strong π–π stacking force exists.[11] Thus, through this specific interaction between the PANI chain and RGO, RGO could induces more expanded coil conformation in the PANI chains with the help of the abundant graphitic surface of reduced graphene oxide (RGO). In addition to the enhanced electrical conductivity of the film, reinforced mechanical properties arising from the RGO could also be expected.[12] There have been many papers on incorporating various carbon materials with PANI for the electrodes of supercapacitors;[5c,d,11c,12a,b,13] however, research dealing with RGO as an inducer for expanding the molecular conformation of PANI chains in solution has rarely been reported. The most interesting point of this research is that RGO affects the molecular conformation of PANI chains, which helps the PANI/RGO hybrid film reach an electrical conductivity greater than both RGO and PANI components. This is because the composite materials, which consist of two materials with different electrical properties, usually possess an electrical conductivity between the two each component. In this work, PANI/RGO films were prepared with different weight percentages of PANI (88, 76, and 60%), and two different sizes were prepared depending on the size of the substrate (8 and 13 inch). The produced films were characterized by Raman spectroscopy, XPS, XRD, and direct-current electrical measurements to systematically investigate the effect of RGO in determining the conformation of PANI chains and overall crystalline structure and electrical conductivity of the films. Electrochemical measurements, involving cyclic voltammetry (CV) and galvanostatic tests were also performed to investigate the potential of the PANI/RGO film to be used as an electrode material for scalable and flexible supercapacitors.

2. Results and Discussion

2.1. Fabrication of Re-Doped PANI/RGO Hybrid Film

Figure 1 shows a schematic illustration of the synthetic procedure of PANI/RGO film. First, the RGO powder was added to HCl solution and sonicated for 24 h to obtain homogeneous dispersion. Then aniline monomer was added, keeping vigorous stirring. After stirring the above solution for 1 h, chloroform was mixed to prevent the freezing of the reaction solution. When the temperature of the solution decreased to –9 °C in the chiller, the anilinium hydrochloride became partially insoluble in the aqueous phase and co-existed in both the aqueous and organic phase.[10] Thus, the hydrophobic part of the anilinium hydrochloride (phenyl group) adsorbed on the aromatic surface of the RGO by the π–π interaction in the organic phase.[11a] After addition of initiator, ammonium persulfate (APS), the polymerization of aniline occurred on the surface of the RGO, and then PANI emeraldine salt (ES)/RGO (PARG) was obtained. After washing and drying, the primary dopant of PANI ES in PARG was removed by ammonia solution, resulting in de-doped PARG (De-PARG). After additional washing and drying, De-PARG was re-doped by CSA, and then re-doped PARG (Re-PARG) was dissolved in m-cresol/chloroform solvent. This secondary doping process is very helpful in changing the conformation of PANI chains from a compact coil to an expanded structure in the solvent.[6d] Furthermore, it is expected that RGO also induced

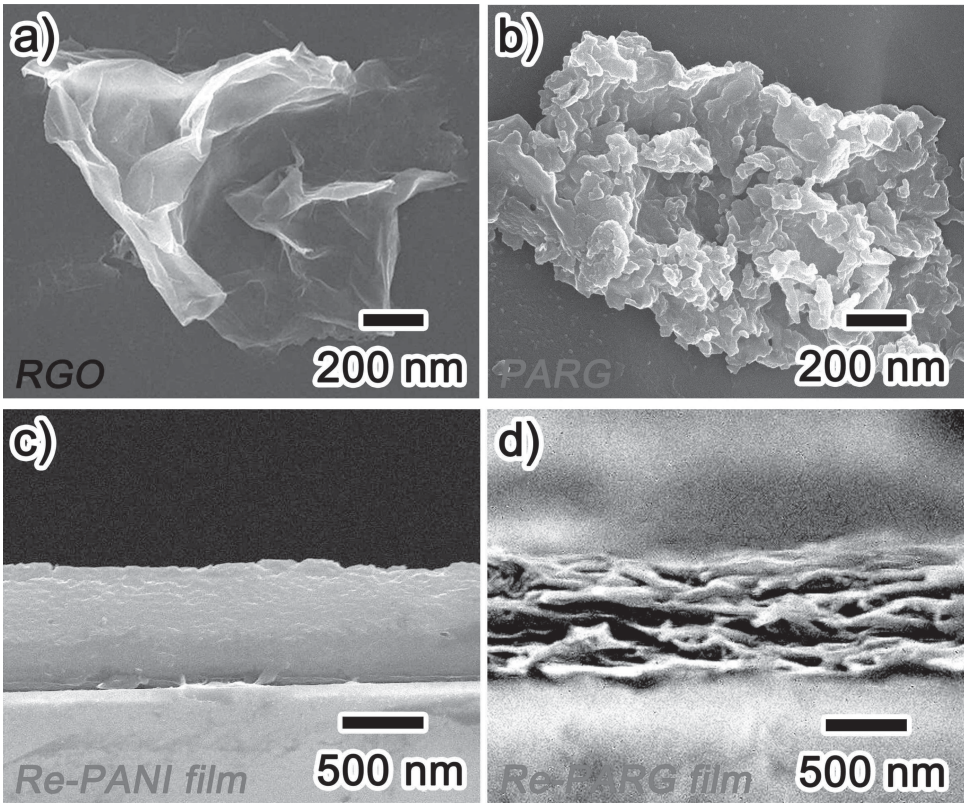

Figure 2. SEM images of a) pristine RGO, b) PARG, c) cross-sectional view of Re-PANI film, and d) Re-PARG film.

the more expanded coil conformation of PANI chains in the solution via strong π–π interactions between the quinoid rings of the PANI chains and the basal planes of RGO. Finally, the prepared solution was cast onto a large-sized glass substrate (23 cm × 23 cm, 13 inch) and placed on a heat source to evaporate any residual solvent. Due to the high surface polarity and wettability of the m-cresol solvent, the prepared solution was well attached to the glass substrate.[6d,14] After the annealing process, as shown in the last picture of Figure 1, we obtained the large-scale Re-PARG film (23 cm × 23 cm, 13 inch). Additionally, we were able to fabricate the smaller sized film (16 cm × 13 cm, 8 inch) easily by changing the size of the glass substrate (Figure S1, Supporting Information), demonstrating the great advantage of the solution process for producing the scalable film.

2.2. Characterization of Re-Doped PANI/RGO Hybrid Film

Figure 2a–d illustrate the SEM images of pristine RGO, PARG, re-doped PANI (Re-PANI) film, and Re-PARG film, respectively. As shown in Figure 2a, pristine RGO exhibits the wrinkled and silk-like structure related with the intrinsic characteristics of graphene.[12a,15] The TEM images of RGO (Figure S2a, Supporting Information) additionally show the thin and transparent two-dimensional morphology with the size of several micrometers, suggesting that few layers of RGO were utilized to synthesize the Re-PARG film. The SEM and TEM images of the PARG (Figure 2b and Figure S2b, Supporting Information) clearly show that the PANI was uniformly and successfully polymerized on the surface of the few micrometer sized-RGO, which could be beneficial for the homogeneous dispersion of the Re-PARG in the solution. The cross-sectional image of the Re-PARG film (Figure 2d) clearly shows that the RGO components are laterally intercalated with the PANI component, while the Re-PANI film displays a relatively smooth cross-section (Figure 2c). The RGO-intercalated structure of the Re-PARG film is probably attributable to the homogeneous dispersion of the Re-PARG in the solution and the strong π–π interactions between the graphitic surface of the RGO and the quinoid rings of the PANI backbone.

Raman spectroscopy was used to analyse the structural changes of the PANI component during de-doping and re-doping processing and to measure the vibrational spectra of nonpolar bonds, such as carbon–carbon interactions between the PANI backbone and the basal planes of RGO. The Raman spectra of the graphite oxide (GO), RGO, Re-PARG film, De-PARG, PARG, and PANI (ES state) samples are shown in **Figure 3**a (the important peaks are marked with black dots). As shown in Figure 3a, structural changes occurred during the chemical processing from GO to RGO in the exfoliation/reduction step and during the transition of PARG to Re-PARG film in the de-doping/re-doping process. Both GO and RGO display the two prominent Raman-active peaks at 1330 cm^{-1} assigned to the D mode corresponding to the structural defects and at 1590 cm^{-1} corresponding to the G mode related

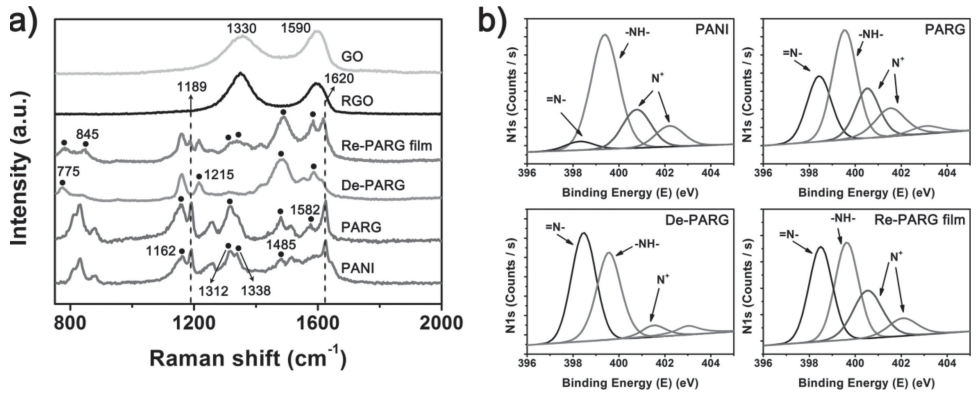

Figure 3. a) Raman spectra of GO, RGO, Re-PARG film, De-PARG, PARG, and PANI (ES state), b) N 1s XPS spectra of PANI (ES state), PARG, De-PARG, and Re-PARG film.

to the first-order scattering of the E_{2g} mode observed for sp^2-carbon domains.[12b,16] The Raman spectra of RGO exhibit the increased intensity ratio of the D band to G band (I_D/I_G) compared to that of GO, suggesting that the reduction process increased the defect content or edge area in RGO sheets.[12b] In addition to the reduction process, the decreased size of the graphene sheets might also cause the structural defect, leading to an increase of I_D/I_G.[12a,b] The Raman spectra of pure PANI show the distinctive vibrations of C–C stretching of the para-distributed benzenoid ring, C=N stretching of the quinoid ring, C=N stretching of the quinoid ring, C–$N^{\bullet+}$ stretching in polaron form (cationic amine units of the benzenoid ring), C–N^+ stretching in bipolaron form (cationic imine units of the quinoid ring), C-N stretching, C-H bending of the benzenoid ring, C-H bending of the quinoid ring, benzenoid ring deformation, and C–H bending of the quinoid ring and quinoid ring deformation at 1620 cm^{-1}, 1513 cm^{-1}, 1485 cm^{-1}, 1338 cm^{-1}, 1312 cm^{-1}, 1255 cm^{-1}, 1189 cm^{-1}, 1162 cm^{-1}, 878 cm^{-1}, and 832 cm^{-1}, respectively.[12b,17] These peaks show the coexistence of quinoid and benzenoid structures in PANI ES. After aniline monomers were polymerized on the RGO, the PARG presented four distinguishable peaks that differed from those seen in pure PANI: Increase in the intensity of quinoid ring-related vibrations at 1485, 1312, and 1162 cm^{-1} corresponding to the C=N stretching of the quinoid ring, C–N^+ stretching in bipolaron form and C–H bending of the quinoid ring, and appearance of the C=C stretching vibrational mode of the quinoid ring at 1582 cm^{-1}.[17c] These peaks in the PARG probably result from the strong inter-molecular π–π stacking, which causes the overlapping of P_z orbitals between the basal planes of the RGO and the quinoid rings of the PANI backbone.[11b] Thus, it can be assumed that the aniline monomers were successfully polymerized on the RGO via the strong π–π stacking between RGO and PANI. In the Raman spectra of De-PARG, the peaks of C–$N^{\bullet+}$ and C–N^+ corresponding to 1338 and 1312 cm^{-1} almost disappeared, whereas the peaks at 1215 and 775 cm^{-1} were newly appeared. The vibrational bands at 1215 and 775 cm^{-1} were attributed to C–N stretching in the emeraldine base (EB) form of PANI and quinoid ring deformation.[17b,18] Additionally, it was also observed that the peak at 1620 cm^{-1} corresponding to the C–C stretching of the para-distributed benzenoid ring significantly decreased, while the C=C stretching band of the quinoid ring and the C=N stretching vibration of the quinoid ring, corresponding to 1582 cm^{-1} and 1485 cm^{-1}, increased considerably. The EB form of PANI is known to have a higher imine/amine and quinoid ring/benzenoid ring ratio than the ES form.[6d,12b,19] Moreover, it should also be noted that PANI ES significantly losses its bipolaronic and polaronic structure by de-protonation.[12b,20] Consequently, with the emergence of the new vibration related with the EB form of PANI (1215 cm^{-1}), the observed peaks in De-PARG clearly reveal that the ES state of PANI on the RGO turned to the EB state by the de-doping process. After De-PARG was re-doped by CSA, four different features appeared in the spectra of Re-PARG film: 1) re-emerged bands of the bipolraon and polaron form and C–H bending of the benzenoid ring at 1310–1340 and 1189 cm^{-1}; 2) new appearance of an amine deformation peak at 845 cm^{-1}; 3) increase in the intensity of the C–C stretching vibrational mode of the para-distributed benzenoid ring and the C=C stretching band of the quinoid ring at 1620 and 1582 cm^{-1}; 4) up-shifted peaks of the C=N stretching of the quinoid ring and quinoid ring deformation at 1489 and 782 cm^{-1} from the peaks at 1485 and 775 cm^{-1}. The re-emerged benzenoid ring peak (1189 cm^{-1}), newly appeared amine deformation peak (845 cm^{-1}),[17a] and increased benzenoid ring peak (1620 cm^{-1}) obviously reflect the increased doping level of PANI in the Re-PARG film. Additionally, the re-emerged bipolraon and polaron bands provide crucial evidence of the successful re-protonation of the PANI component in the Re-PARG film. Thus, it can be assumed that the up-shift of the two quinoid ring vibrations at 782 and 1489 cm^{-1} can be attributed to the changed backbone structures of PANI in the Re-PARG film. It is known that the quinoid ring and imine nitrogen atoms in the PANI backbone are substantially converted to benzenoid ring and amine nitrogen atoms when the EB state of the PANI turns to the ES state.[6d,19b,c] However, the quinoid ring vibrations at 1582, 1489, 1162, and 782 cm^{-1} did not disappear even after the re-doping process, but dominated the overall Raman spectrum of the Re-PARG film. Furthermore, the peak at 1582 cm^{-1} corresponding to the C=C stretching band of the quinoid ring was slightly increased. As described above, the graphitic surface of the RGO interacts strongly with the quinoid ring of the PANI

through the π–π stacking. Consequently, the overlapping of the P_z orbitals of the quinoid rings of the PANI with the aromatic surface of RGO would result in the strong quinoid ring peaks in the Re-PARG film.

XPS analysis was also conducted to investigate the structural change of PANI in the de-doping/re-doping process and the specific interaction between RGO and the PANI backbone (Figure 3b). In this study, N1s spectra of PANI (ES state), PARG, De-PARG, and Re-PARG film samples were collected. In the N1s spectra of PANI sample, the peak at 398.5 eV (black line) corresponds to quinoid imine (–N=), and the more prominent peak at 399.5 eV (red line) corresponds to benzenoid amine (–NH–) in the PANI backbone.[21] An additional two minor peaks at 400.8 eV and 402.2 eV (blue and dark cyan lines) correspond to positively charged imine in the bipolaron state and protonated amine in the polaron state.[22] These spectra demonstrate the typical structure of the PANI in ES form.

After the polymerization of PANI on RGO, some structural changes were observed in the PARG. Increased XPS peak signal area of the quinoid imine peak at 398.4 eV, from 0.38% of the overall PANI signal area to 1.57% of the PARG signal area, was observed. The peak at 400.5 eV, which represents charged imine, is also slightly increased. The strong π–π stacking between the PANI backbone and RGO might have caused an increase in the quinoid imine peaks.

The N1s spectra of De-PARG sample shows increased peak at 398.5 eV and diminished peak at 399.5 eV, which correspond to quinoid imine and benzenoid amine in the backbone, while only one minor peak at 401.5 eV for the protonated amine part[12b] is shown. Increased imine peak is due to the ammonium hydroxide addition and following de-protonation of amine in the PANI ES backbone.[6d,12b,19] Additionally, when the ES form of PANI changed to the EB form, it possessed almost no charge in the backbone,[12b,20] resulting in the disappearance of the positively charged imine peak at 400.5 eV and the attenuated peak of protonated amine at 401.5 eV.

After De-PARG was re-doped by CSA, the XPS analysis on the Re-PARG film suggests that the charged bipolaron structure (re-emerged blue peak at 400.5 eV) and polaron structure (increased dark cyan peak at 402.2 eV) were restored. Thus, it could be assumed that the ES form of the PANI backbone was successfully re-established.[20a,23] The re-doping of the EB state of PANI is known to induce a substantial transition of imine nitrogen atoms to amine nitrogen atoms in the PANI backbone.[6d,19b,c] However, the quinoid imine (–N=) peak at 398.5 eV considerably remained even after the re-doping process. Therefore, this result suggests that the specific π–π interaction between the quinoid ring of the PANI and the graphitic surface of the RGO exists and the interaction leads to preservation of the quinoid imine structure in the Re-PARG sample, which is in accordance with the previous Raman analysis.

As described above, it has been found that PANI chains re-doped by CSA could change their molecular conformation possessing the mobility with its counter-ion in the m-cresol/chloroform co-solutions.[6d] Additionally, it is known that when the interaction between polymer and solvent is larger than the interaction between polymer and polymer, more linear polymer chain conformation is preferred due to the increased possibility that the polymer chains will interact with the solvent.[6d] Thus, considering these facts, it is expected that the strong interaction between the PANI and RGO (π–π interaction) effectively helps PANI chains possess the more linear conformation, leading to increased crystallinity along with improved electrical conductivity. In the next step, we measure the electrical conductivity and crystalline structure of the films to achieve an in-depth insight into the role of the RGO in determining the conformation of PANI chains and overall crystalline structure and electrical conductivity of the films.

2.3. Effect of RGO in Determining Crystalline Structure and Electrical Conductivity of Re-Doped PANI/RGO Hybrid Film

In order to elucidate the role of the RGO in determining the electrical properties and crystalline structure of the composite film, the De-PARG samples (De-PARG 1–3) were first prepared with various mass ratio of de-doped PANI (De-PANI) to RGO. The prepared De-PARG 1–3 samples were used in producing the Re-PARG 1–3 films without any weight ratio change of either component. Thermo-gravimetric analysis (TGA) was performed to assess the precise weight percentages of the PANI component in the De-PARG 1–3 samples under air flow at a heating rate of 10 °C min^{-1} (detailed description in Figure S3, Supporting Information). Based on these TGA data, the weight percentage of PANI component was calculated as 88, 76 and, 60% for De-PARG 1, 2, and 3, respectively. The four-probe method was conducted to measure the electrical conductivity of the samples. The Re-PANI film and RGO were prepared as control materials. **Figure 4**a presents the electrical conductivities of the Re-PARG films and control samples. The electrical conductivities of Re-PANI film, Re-PARG 1 film, Re-PARG 2 film, Re-PARG 3 film, and RGO were measured as ≈580, 762, 906, 298, and 46.5 S cm^{-1}, respectively. Starting from the Re-PANI film, the electrical conductivity of the film increased to the maximum of 906 S cm^{-1} (Re-PARG 2 film) as the weight percentage of the RGO increased to 24%, while decreased value of conductivity was measured in Re-PARG 3 film. Additional TGA and XRD analysis were conducted to measure the remaining solvent in the film and ascertain the effect of the solvent evaporation on the electrical performance of the film over time. The as-prepared Re-PARG 2 film and Re-PARG 2 film after keeping for 150 days were used in both TGA and XRD analysis and the Re-PARG 2 powder before mixing with m-cresol and chloroform was used as a control in TGA test (detailed description in Figure S4, Supporting Information). The weight percentage of remaining solvent in the as-prepared Re-PARG 2 film and the Re-PARG 2 film after keeping for 150 days were measured to be as ≈1.25 wt% and ≈0 wt%, indicating that negligible amount of solvent was remained on the film after annealing process and solvent evaporation is occurred with time. The XRD analysis illustrates that enhanced crystalline structure of the film was maintained even after storing for 150 days. Therefore, it is considered that crystalline structure was not affected by solvent evaporation and performance of the material is well maintained over time.

Figure 4b shows the XRD patterns of the graphite, GO and RGO. The XRD pattern of graphite presented a typical (002) narrow peak[24] at 2θ = 26.5°, corresponding to a d-spacing

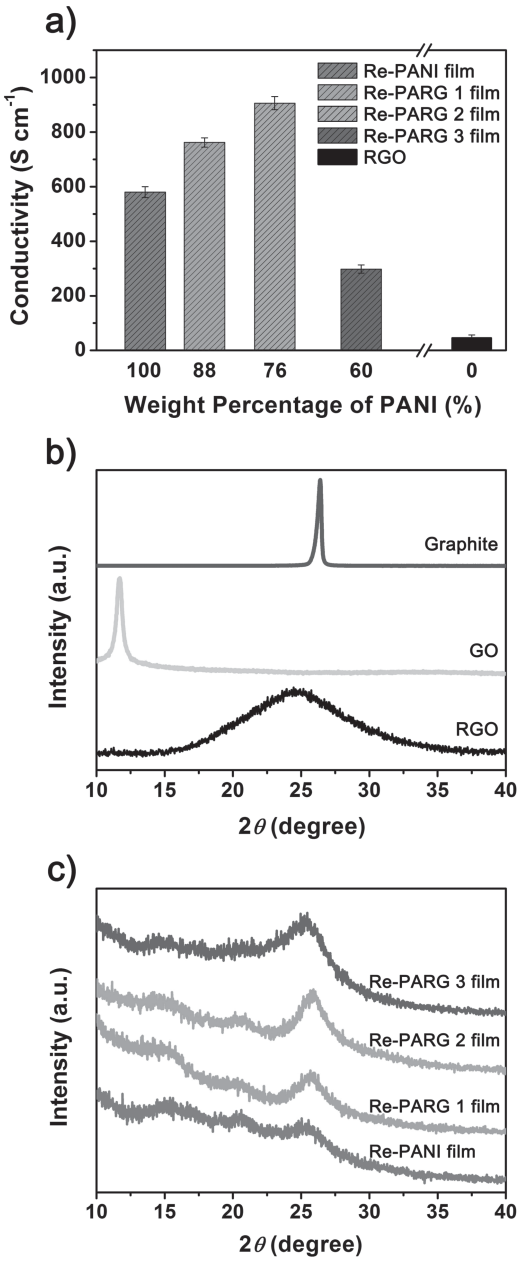

Figure 4. a) Electrical conductivity of Re-PANI film, Re-PARG 1–3 films, and RGO displayed as function of the weight percentage of PANI component; b) XRD patterns of graphite, GO, and RGO; c) XRD patterns of Re-PARG 1–3 films and Re-PANI film.

of ≈3.36 Å. In the case of GO, a sharp diffraction peak was observed at $2\theta = 11.65°$ (d-spacing ≈ 7.59 Å), which can be assigned to the (001) reflection peak.[12a] The increase in the interlayer distance from ≈3.36 Å for graphite to ≈7.59 Å for GO reflects successful oxidation of graphite.[16] After ultrasonication and reduction steps, the (001) reflection peak of GO disappeared, and one broad peak centered at 24.58° (d-spacing ≈ 3.62 Å) appeared in the XRD spectra of RGO, illustrating that the GO was efficiently reduced into RGO.[13a]

Figure 4c represents the XRD patterns of Re-PARG 1–3 films and Re-PANI film. The Re- PANI film shows three peaks centered at $2\theta = 15.3°$, 20.5°, and 25.6° (d-spacings ≈ 5.8, 4.3, and 3.5 Å) on the broad background, revealing the semi-crystalline nature of the PANI. By increasing the weight percentage of RGO from 0% (Re-PANI film) to ≈12% (Re-PARG 1 film), the peaks at 15.3° and 20.5° decreased along with the decrease in the broad background, whereas the peak at 25.6° increased. When the weight percentage of RGO reached 24% (Re-PARG 2 film), with the maximum electrical conductivity (906 S cm^{-1}) among the films, the peaks at 15.3°, 20.4° and the broad background mostly disappeared and the diffraction pattern of the Re-PARG 2 film was dominated by the peak at 25.6°. This indicates an increase in the crystalline phase of the film and strengthened stacking along the specific direction. More specifically, these results have following three implications. First, the disappearance of the intrinsic peak of RGO (24.58°) in the XRD patterns of the Re-PARG 1 and 2 films clearly indicates that the RGO is properly intercalated into PANI chains. Second, it is known that the d-spacing of ≈3.5 Å (25.6°) is the face-to-face π–π stacking distance between neighboring phenyl rings in the crystalline structure of the PANI.[25] Thus, the increase in the intensity of the peak at 25.6° along with the decrease in the intensity of the peaks at 15.3°, 20.5° and the broad background reflect that π–π inter-chain stacking between the phenyl rings of the PANI chains was intensified. Third, based on the strengthened peak (25.6°) of the Re-PARG 1 and 2 films with the increase of RGO contents, it is considered that the basal planes of RGO and phenyl rings also form π–π stacking with a distance of 3.5 Å. Considering these results, the mechanism of improved electrical conductivity of Re-PARG 1 and 2 films could be explained in the following manner: The chemical structure of the micro-meter sized RGO consists of a number of aromatic rings. Thus, when PANI and RGO co-exist in the solution, it is expected that the PANI chains would strongly interact with the aromatic structure of RGO by the π–π overlapping of the basal planes of the RGO and the quinoid rings of the PANI, resulting in more expanded coil conformation of the PANI chains. Then, the PANI chains expanded by the RGO would induce more planar stacking with nearby PANI chains sequentially. In this way, the PANI chains would form the more planar chain conformation and compact packing structure. This compact packing of PANI chains would inhibit the considerable ring rotations (π–conjugation defects) of the phenyl rings from the plane of the backbone, leading to the improved π–π interactions, extensive three-dimensional delocalization of charge, and increase in the crystallinity and electrical conductivity.[6d,23] This compact crystalline structure of PANI chains with RGO is proposed as a pictorial scheme in Figure S5 (Supporting Information) where PANI chains are located between RGO.

However, as the weight percentage of RGO further increase to 40% in the Re-PARG 3 film, the XRD pattern showed an increase in broad background, re-emerged peaks at 15.3° and 20.5°, and a weak change in peak intensity at 25.6°. This indicates that an overall decrease in the crystallinity of the film has occurred, and the PANI chains are not aligned in one direction after the specific weight percentage of RGO (40%). Based on the highly disordered crystalline structure of the pristine RGO

(Figure 4b), the increase in the amorphous region in the Re-PARG 3 film is considered as a result of the increased influence of the poorly ordered structure of the RGO. This increase in the amorphous region of the film would result in a shorter mean free path and worsened carrier transport, leading to the decrease in the electrical conductivity of the film.[6e,25b] Consequently, the XRD analysis demonstrates that RGO in the composite favorably or unfavorably changes the crystalline structure of PANI depending on PANI/RGO weight ratios, leading to the increase or decrease in the electrical conductivities of PANI/RGO hybrid films. Most interesting part of XRD analysis is that the strong π–π interactions of RGO with the quinoid rings of the PANI chains increase the electrical conductivity and crystallinity of the PANI/RGO hybrid film, which is greater than both RGO and PANI. To investigate the advantages of enhanced electrical conductivity and crystallinity of Re-PARG film as a supercapacitor electrode, electrochemical analysis was performed to the Re-PARG 2 film.

2.4. Electrochemical Performance of Re-Doped PANI/RGO Hybrid Film

CV and galvanostatic charge/discharge analysis were conducted in 1 M H_2SO_4 electrolyte with three-electrode system to evaluate electrode performance. For a comparison, the Re-PANI film and pristine RGO were also used as electrodes for supercapacitor. **Figure 5**a illustrates the CV curves of the Re-PARG film, Re-PANI film and RGO at a scan rate of 5 mV s^{-1} from 0 to 0.8 V. The CV curve of RGO shows the rectangular shape without any redox peaks, reflecting the good charge propagation and electrical double layer (EDL) capacitance of the carbon materials.[12b,13a,b] On the contrary, two pairs of broad redox peaks were observed for the Re-PARG and Re-PANI films, revealing the existence of the pseudo-capacitive PANI component in the Re-PARG film.[12b] The two observed redox peaks originated from its redox transitions between the leucoemeraldine form (semiconducting state), the ES form (conducting state) and the Faradic transformation of emeraldine/pernigraniline.[12a,13a,25b] Additionally, the CV curve of the Re-PARG film showed the largest CV loop area with the highest current response, demonstrating the larger specific capacitance of the Re-PARG film than the RGO and the Re-PANI film.[5d,13b] This phenomenon suggests that the RGO in the Re-PARG film is a crucial factor for enhanced capacitance compared with that of the RGO and the Re-PANI film.

To further elucidate the electrochemical behavior of the Re-PARG film, Re-PANI film and RGO, the galvanostatic charge/discharge test was carried out at a current density of 0.45 Ag^{-1} from 0 to 0.8 V in 1 M H_2SO_4 electrolyte. As shown in Figure 5b, the galvanostatic charge/discharge curve of the RGO exhibits a symmetric triangular shape, indicating that its capacitance originates from the EDL capacitance,[5c] as described above. In contrast, the discharge curve of the Re-PARG film exhibits two distinct voltage stages: ≈0.8–0.6 V and ≈0.6–0 V, respectively. The first stage, with a relatively short discharging duration, is attributed to EDL capacitance, whereas the second stage, with a much longer discharging duration, is due to the combination of EDL and faradaic capacitances of the PANI component in the film.[5c] The discharge curve of the Re-PANI film also represents a shape similar to that of the Re-PARG film. However, the Re-PARG film exhibits a much longer discharging time and less vertical voltage drop at the beginning of the discharge curve than the Re-PANI film, indicating that the Re-PARG film possesses much higher specific capacitance and smaller internal resistance than the Re-PANI film.[13c,25b] Possessing low internal resistance as a supercapacitor is a crucial factor for improving the capacitance of the materials and reducing unwanted power consumption.[13d,15]

The precise gravimetric capacitances (Figure 5c) and internal resistances (Figure 5d) of all samples were calculated from the galvanostatic discharge curves[11c,13a] and vertical voltage drop at the initial point of each discharge curve[25b] (Detailed description in experimental section). The RGO, Re-PANI film, and Re-PARG film exhibit the gravimetric capacitances of 50, 256, and 431 F g^{-1} and internal resistances of 0.036, 0.04, and 0.02 Ω g, respectively. The Re-PARG film and the Re-PANI film show much higher gravimetric capacitances than the RGO electrode. Generally, pseudo-capacitance is much higher than EDL capacitance, because pseudo-capacitive materials take advantage of fast redox reactions by utilizing whole mass.[2b,26] Thus, though the RGO displays lower internal resistance than the Re-PANI film electrode, the RGO illustrates the lowest gravimetric capacitance among all the samples due to the absence of pseudo-capacitive materials.[5c] Interestingly, without any specific nanostructure, the Re-PANI film shows a relatively small internal resistance and a high gravimetric capacitance. This high gravimetric capacitance and low internal resistance of the Re-PANI film are perhaps due to its high electrical conductivity,[13b,27] which is one of the highest among those reported in the literature.[6e,10,13b] Notably, when the PANI component is incorporated with the RGO in film form, the Re-PARG film exhibits the highest gravimetric capacitance and the lowest internal resistance among all the samples, indicating the synergistic effect of PANI and RGO. This effect originates from the following two factors: 1) the combining effect of the EDL and faradaic capacitances,[13c,d] in agreement with the two voltage stages of ca. 0.8–0.6 V and 0.6–0 V and 2) the extremely high electrical conductivity[13b] from improved conducting networks of PANI chains by the RGO and the strong π–π interactions between the RGO and the PANI chains. PANI, in its leucoemeraldine or pernigraniline form, is an insulator; accordingly, the supercapacitors possessing the PANI component suffer from large internal resistance, as it is close to the fully charged or discharged state.[5c,12a,13a,25b] However, the Re-PARG film possesses the RGO component, which could act as a good current collector, and the strong π–π interactions between the RGO and the PANI chains in the Re-PARG film could provide a good conducting network even though PANI is close to the insulating form, which facilitates the redox reaction of PANI and leads to the increase in the pseudo-capacitance.[5c,11c,13b] Concurrently, the Re-PARG film with enhanced conducting networks decrease the internal resistance, leading to the improvement in effective energy storage by reducing the energy consumption caused by internal resistance.[13d]

The CV test was also performed on the Re-PARG film of two different sizes in 1M H_2SO_4 at a scan rate of 5 mV s^{-1} (Figure 5e).

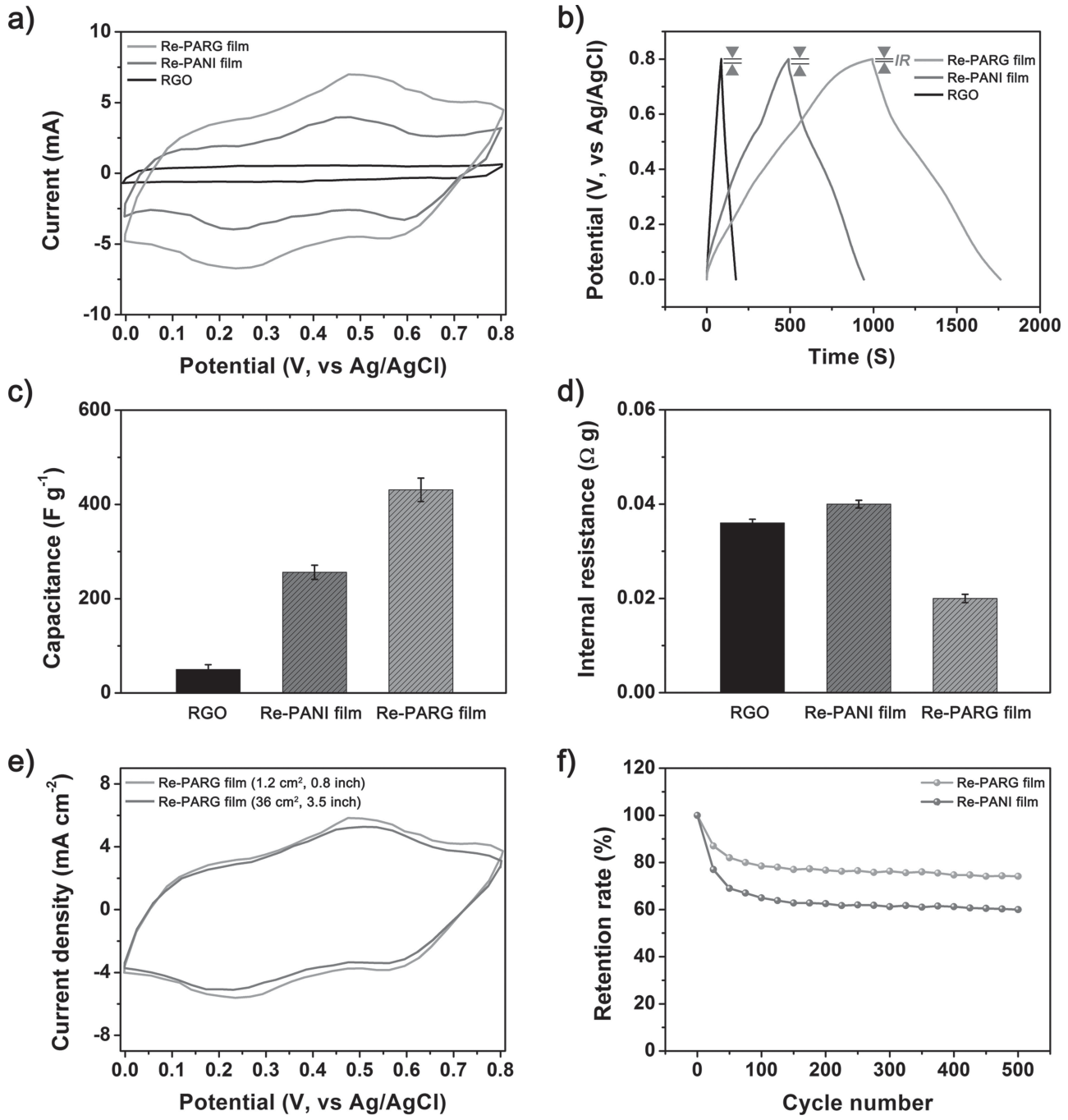

Figure 5. a) CV curves of Re-PARG film, Re-PANI film and RGO electrodes at a scan rate of 5 mV s^{-1} between 0 and 0.8 V in 1M H_2SO_4 solution; b) Galvanostatic charge/discharge curves of Re-PARG film, Re-PANI film and RGO electrodes at current density of 0.45 A g^{-1} in 1 M H_2SO_4 solution; c) Gravimetric capacitances of RGO, Re-PANI film and Re-PARG film electrodes at current density of 0.45 A g^{-1}; d) Internal resistances of RGO, Re-PANI film and Re-PARG film electrodes estimated from the IR drop at a current density of 0.45 A g^{-1}; e) Comparison of CV curves between different sized (1.2 and 36 cm^2) Re-PARG film electrodes at a scan rate of 5 mV s^{-1}; f) Cyclic stability of Re-PARG film and Re-PANI film electrodes as a function of cycle number at a current density of 0.45 A g^{-1}.

The size of one film (36 cm^2, 3.5 inch) was 30 times larger than that of the other one (1.2 cm^2, 0.8 inch). Both films were lightweight (2 and 60 mg) and thin (14.5 μm). Remarkably, even after the size of the film was increased 30 times, the larger sized film demonstrated an area capacitance of 0.655 F cm^{-2} (393 F g^{-1}), which is only 9% smaller than that of the smaller sized film (0.718 F cm^{-2}, 431 F g^{-1}), suggesting a promising electrochemical property for large-scale supercapacitors.

The typical poor long-term stability of supercapacitors based on the CPs during cycling is one of the greatest obstacles in producing

low-cost electrode materials for commercially available supercapacitors.[13f] As shown in Figure 5f, the Re-PANI film shows a rapid initial drop on capacitance retention and maintains 60% of initial gravimetric capacitance (from 256 to 153 F g^{-1}) after 500 charging/discharging cycles at a current density of 0.45 A g^{-1} because PANI suffers from swelling and shrinkage during charging/discharging cycling.[5c,13a,d,f] The capacitance retention of the Re-PARG film also displays a rapid initial drop due to the large portion of PANI component (76 wt%) in the Re-PARG film. However, in the case of the Re-PARG film, it exhibits improved capacitance retention of 74% (from 431 to 318 F g^{-1}) after 500 charging/discharging cycles under the same conditions, due to suppression of the shrinking and swelling of the PANI chains by the mechanically strong RGO.[11c] In addition to the enhanced mechanical property of the film by RGO, the enhanced cycling stability of the film is probably attributed to the increased electrical conductivity of the Re-PARG film. It is known that low electrical conductivity of a device causes the large resistance and joule heating while the device is working, which substantially diminishes the life of the organic device.[6e] Therefore, for the Re-PARG film, increased electrical conductivity would lead to the improved cycling stability of the film by reducing the large resistance and joule heating of the electrode during the charging/discharging cycling. To obtain the film with less initial drops on capacitance retention and more enhanced capacitance retention, following method could be used in current PANI-graphene composite system. It has been reported that improvement in mechanical properties of graphene (e.g., from graphene oxide to reduced graphene oxide) could increase the retention rate of PANI-graphene composite by enhancing the restraint of shrinkage and swelling of PANI chains during charging/discharging processes.[12b] From this point of view, possible improvement can be realized by using mechanically stronger single-layer graphene sheet (e.g., fabricated by chemical vapor deposition or arc-discharge method)[16,28] or graphene nanoribbon[29] than RGO prepared by Hummers' method. The enhanced mechanical resilience by mechanically stronger graphene sheet or graphene nanoribbon might result in cycling performance improvement with the enhanced electrical conductivity and crystallinity due to the π–π stacking between PANI structure and graphitic surface of single-graphene sheet or graphene nanoribbon. Using this method, the cyclability of the PANI-RGO system electrode can probably be increased even in long cycles. Finally, all of these results suggest the great potential of the PANI/RGO film to be used as an electrode material for high-performance scalable supercapacitors.

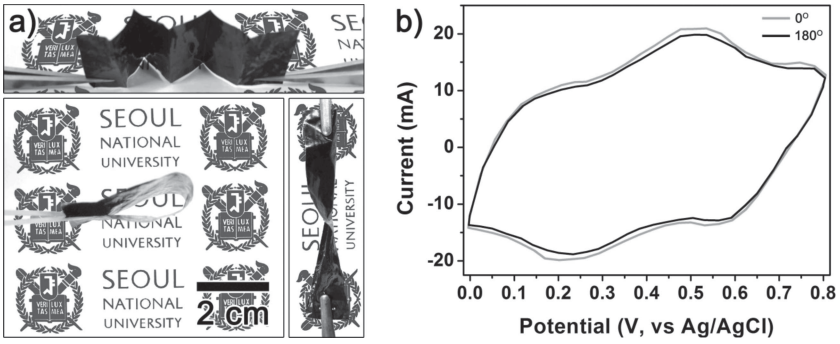

Figure 6. a) Digital photographs of flexible Re-PARG film. The top image exhibits the folding characteristics of the film. The bottom images illustrate the high flexibility (bending and twisting) of the film; b) CV curves of Re-PARG film electrodes with two different bending angles of 0° and 180° at a scan rate of 5 mV s^{-1}.

2.5. Flexibility of Re-Doped PANI/RGO Hybrid Film and Electrochemical Performance of Re-Doped PANI/RGO Hybrid Film under Bending Condition

Figure 6a depicts the great flexibility of the Re-PARG film, which can endure bending, twisting, and even folding without any destruction. This high flexibility of the Re-PARG film is attributed to the inherent flexibility of the CPs.[6e,13b,30] Additionally, in order to test the supercapacitor performance of the Re-PARG film under bending conditions, the CV test was also performed on the films with two different bending angles of 0° and 180° at a scan rate of 5 mV s^{-1}. As shown in Figure 6b, the Re-PARG films represent the non-substantial difference between the CV curves with bending angles of 0° and 180°, indicating the superior performance ability of the Re-PARG film as a flexible supercapacitor. Therefore, the Re-PARG film can potentially be applied in producing flexible electronic equipment such as bendable displays, intelligent clothes, and various flexible devices.

3. Conclusion

In summary, the PANI/RGO hybrid (Re-PARG) film was successfully fabricated through solution processing. The strong π–π interactions of RGO with the quinoid rings of the PANI chains in the solution induced the more expanded conformation of the PANI chains, leading to the extremely high electrical conductivity of the film (906 S cm^{-1}) (greater than the pristine PANI film (Re-PANI film, 580 S cm^{-1}) and RGO (45.6 S cm^{-1})). Additionally, the film demonstrated the high capacitance of 431 F g^{-1}. The Re-PARG film also demonstrated excellent performance ability as a scalable and flexible electrode material for high-performance supercapacitors with various film sizes and even under bending conditions. This approach will offer a valuable and promising tool for producing highly flexible, scalable, and high-performance supercapacitor electrodes.

4. Experimental Section

Preparation of Re-PARG Films: Materials needed and methods for preparation of the RGO is described in supporting information. The as-prepared RGO powder was added to HCl solution (2.5 M, 40 mL) in Erlenmeyer flask. The solution was sonicated for 24 h and aniline monomer was added, keeping vigorous stirring. After that, chloroform (60 mL) was added to the mixture, leading to the phase separation (chloroform phase at the bottom, aqueous phase on the top). Then the initiator, APS (the weight ratio of APS : aniline = 1.2:1)

in HCl solution (3.75 M, 16 mL), was added to the above bi-phase solution and stirred for 24 h at –40 °C, resulting in the low-temperature interfacial polymerization. After polymerization process, the solution was centrifuged and dried. The feeding weight ratio of aniline to RGO was changed as 16:1, 12:1, and 8:1, and the obtained composites were named as PARG 1, PARG 2, and PARG 3, respectively. The PARG powder was dispersed in ammonia solution (1.2 M, 215 mL) and vigorously stirred for 24 hr to de-dope the PANI chains on the RGO, resulting in the De-PARG. This solution was centrifuged again and dried to collect powder. The real weight percentages of the PANI component in the De-PARG 1, 2, and 3 composites were calculated as 88% for De-PARG 1, 76% for De-PARG 2, and 60% for De-PARG 3, respectively. The De-PARG powder was mixed with the CSA (the mole ratio of PANI : CSA = 2:1) to re-dope the PANI chains on RGO, resulting in the Re-PARG. The Re-PARG powder was added to the m-cresol/chloroform solution (the volume ratio of m-cresol : chloroform = 7:3) to be as 2.38 wt% of total mass of solution and stirred for 3 h and sonicated for 24 h. The Re-PARG solution was drop-casted onto glass substrate and was annealed at 40 °C for 16 h. Finally, the free standing film was obtained by detaching the annealed film from the glass substrate in the water. The Re-PARG films which were prepared by the De-PARG 1, 2, and 3 were named as the Re-PARG film 1, 2, and 3, respectively. The synthetic procedures of the PANI (ES state), De-PANI (EB state), and Re-PANI film were identical to those of the PARG, De-PARG, and Re-PARG film except incorporation of the RGO.

Characterization: Scanning electron microscope (SEM) and transmission electron microscope (TEM) images were obtained with a JSM-6701F (JEOL, Japan) and LIBRA 120 (Carl Zeiss, Germany), respectively. Raman spectra were recorded using a Horiba-Jobin Yvon LabRam Aramis spectrometer with a 514 nm Ar-ion laser as the excitation source. The X-ray photoelectron spectra (XPS) were collected on Sigma probe (ThermoVG, U.K). Thermo-gravimetric analysis (TGA) was performed on a Perkin Elmer Pyris 6 TGA analyzer (USA) with a heating rate of 10 °C min^{-1} under air flow of 20 mL min^{-1}. The direct-current electrical conductivity measurements of samples were carried out with the four-probe method using a KEITHLY 2400 (KEITHLY, USA). The X-ray diffraction (XRD) patterns were taken with a D8 Advance (Bruker, Germany) equipped with Ni-filtered Cu Kα radiation source (λ = 0.15406 nm).

Electrochemical Measurements: The CV and galvanostatic charge/discharge tests were performed on a Wonatech WBCS 3000 potentiostat/galvanostat instrument to assess the electrochemical performances of the samples. All of the electrochemical measurements were performed in a three-electrode system in H_2SO_4 solution (1 M) as the electrolyte at 25 °C, where the counter and reference electrodes were Pt and Ag/AgCl, respectively. The potential ranges for CV and galvanostatic charge/discharge tests were 0.0 to 0.8 V. The Re-PARG film and Re-PANI film were directly employed as the working electrodes. The pristine RGO was prepared for the working electrode as follows. The mixtures of the RGO (95%) and PTFE (5%) were coated onto the stainless steel mesh (1 cm × 1 cm) and then dried in air at 25 °C for 24 h. The electrochemical behavior was first characterized by the CV test at a scan rate of 5 mV s^{-1}. After that, the galvanostatic charge/discharge test was carried out at a current density of 0.45 A g^{-1} to precisely evaluate the gravimetric capacitance, C_m (F g^{-1}), and internal resistance, R (Ω g). The mass of the Re-PARG film, Re-PANI film, and RGO for the CV and galvanostatic charge/discharge tests were 2 mg. The gravimetric capacitances (C_m) were calculated by using the equation $C_m = (i \times \Delta t)/(m \times \Delta V)$, where C_m is the gravimetric capacitance in F g^{-1}, i is the constant discharge current in mA, Δt is the discharge time in seconds, m is the total mass of the active material in mg, ΔV is the potential window in V. The internal resistances (R) were estimated according to the $R = \Delta V/(i/g)$, where, R is the internal resistance in Ω g, ΔV is the "IR drop (vertical voltage drop at the beginning of the discharge curve)" in V and (i/g) is the discharge current density in A g^{-1}. In order to study the electrochemical performance of the Re-PARG film depending on the size, the CV test was performed to the 2 and 60 mg of the Re-PARG film with the two different sizes (1.2 and 36 cm^2) in H_2SO_4 (1 M) solution at the scan rate of 5 mV s^{-1}. The area capacitances, C_{area} (F cm^{-2}), were calculated according to the following equation from the CV curves $C_{area} = (\int i dV)/(\nu \times \Delta V)$, where C_{area} is the area capacitance in F cm^{-2}, i is the response current density during the discharging in A cm^{-2}, ν is the scan rate in V s^{-1}, and ΔV is the potential window in V. The cycle stability of the Re-PARG film (2 mg) and Re-PANI film (2 mg) were measured by the galvanostatic charge/discharge test at a current density of 0.45 A g^{-1} in H_2SO_4 solution (1 M). For investigating the supercapacitor performance of the Re-PARG film under bending condition, the CV test was performed to the 6 mg of the Re-PARG films with two different bending angles of 0° and 180° at a scan rate of 5 mV s^{-1}.

Supporting Information

Supporting Information is available from the Wiley Online Library or from the author.

Acknowledgements

M.K. and C.L. contributed equally to this work.

Received: September 23, 2013
Revised: November 8, 2013
Published online: December 20, 2013

[1] a) J. R. Miller, P. Simon, *Science* **2008**, *321*, 651; b) X. Lu, Y. Xia, *Nat. Nanotechnol.* **2006**, *1*, 163; c) C. Meng, C. Liu, L. Chen, C. Hu, S. Fan, *Nano Lett.* **2010**, *10*, 4025; d) J. A. Rogers, Y. Huang, *PNAS* **2009**, *106*, 10875; e) D. W. Wang, F. Li, J. Zhao, W. Ren, Z. G. Chen, J. Tan, Z. S. Wu, I. Gentle, G. Q. Lu, H. M. Cheng, *ACS Nano* **2009**, *3*, 1745.

[2] a) H. Nishide, K. Oyaizu, *Science* **2008**, *319*, 737; b) P. Simon, Y. Gogotsi, *Nat. Mater.* **2008**, *7*, 845.

[3] a) Y. He, W. Chen, X. Li, Z. Zhang, J. Fu, C. Zhao, E. Xie, *ACS Nano* **2013**, *7*, 174; b) M. Jin, G. Han, Y. Chang, H. Zhao, H. Zhang, *Electrochim. Acta* **2011**, *56*, 9838.

[4] X. Lu, T. Zhai, X. Zhang, Y. Shen, L. Yuan, B. Hu, L. Gong, J. Chen, Y. Gao, J. Zhou, Y. Tong, Z. L. Wang, *Adv. Mater.* **2012**, *24*, 938.

[5] a) X. Yan, Z. Tai, J. Chen, Q. Xue, *Nanoscale* **2011**, *3*, 212; b) C. Meng, C. Liu, S. Fan, *Electrochem. Commun.* **2009**, *11*, 186; c) Q. Wu, Y. Xu, Z. Yao, A. Liu, G. Shi, *ACS Nano* **2010**, *4*, 1963; d) X. Yan, J. Chen, J. Yang, Q. Xue, P. Miele, *ACS Appl. Mater. Interfaces* **2010**, *2*, 2521.

[6] a) G. Gustafsson, Y. Cao, G. M. Treacy, F. Klavetter, N. Colaneri, A. J. Heeger, *Nature* **1992**, *357*, 477; b) M. Reghu, Y. Cao, D. Moses, A. Heeger, *Phys. Rev. B* **1993**, *47*, 1758; c) S. Cho, S. H. Hwang, C. Kim, J. Jang, *J. Mater. Chem.* **2012**, *22*, 12164; d) A. G. MacDiarmid, A. J. Epstein, *Synth. Met.* **1994**, *65*, 103; e) B. H. Lee, S. H. Park, H. Back, K. Lee, *Adv. Funct. Mater.* **2011**, *21*, 487.

[7] a) J. Jang, J. Ha, J. Cho, *Adv. Mater.* **2007**, *19*, 1772; b) S. J. Yoo, J. Cho, J. W. Lim, S. H. Park, J. Jang, Y. E. Sung, *Electrochem. Commun.* **2010**, *12*, 164; c) K. Y. Shin, S. Cho, J. Jang, *Small* DOI: 10.1002/smll.201203204; d) Y. Kang, M. H. Lee, S. B. Rhee, *Synth. Met.* **1992**, *52*, 319.

[8] a) Y. H. Kim, C. Sachse, M. L. Machala, C. May, L. Müller-Meskamp, K. Leo, *Adv. Funct. Mater.* **2011**, *21*, 1076; b) Y. Xia, J. Ouyang, *J. Mater. Chem.* **2011**, *21*, 4927; c) C. Yu, K. Choi, L. Yin, J. C. Grunlan, *ACS Nano* **2011**, *5*, 7885; d) C. C. Chen, L. Dou, R. Zhu, C. H. Chung, T. B. Song, Y. B. Zheng, S. Hawks, G. Li, P. S. Weiss, Y. Yang, *ACS Nano* **2012**, *6*, 7185.

[9] a) D. Verma, V. Dutta, *Sens. Actuator B-Chem.* **2008**, *134*, 373; b) S. H. Park, K.-H. Shin, J.-Y. Kim, S. J. Yoo, K. J. Lee, J. Shin,

J. W. Choi, J. Jang, Y.-E. Sung, *J. Photochem. Photobiol. A-Chem.* **2012**, *245*, 1.

[10] S. H. Lee, D. H. Lee, K. Lee, C. W. Lee, *Adv. Funct. Mater.* **2005**, *15*, 1495.

[11] a) M. Ginic-Markovic, J. G. Matisons, R. Cervini, G. P. Simon, P. M. Fredericks, *Chem. Mater.* **2006**, *18*, 6258; b) S. Bourdo, Z. Li, A. S. Biris, F. Watanabe, T. Viswanathan, I. Pavel, *Adv. Funct. Mater.* **2008**, *18*, 432; c) X. Lu, H. Dou, S. Yang, L. Hao, L. Zhang, L. Shen, F. Zhang, X. Zhang, *Electrochim. Acta* **2011**, *56*, 9224.

[12] a) N. A. Kumar, H.-J. Choi, Y. R. Shin, D. W. Chang, L. Dai, J.-B. Baek, *ACS Nano* **2012**, *6*, 1715; b) H. Wang, Q. Hao, X. Yang, L. Lu, X. Wang, *Nanoscale* **2010**, *2*, 2164; c) C. N. Rao, A. K. Sood, K. S. Subrahmanyam, A. Govindaraj, *Angew. Chem. Int. Ed. Engl.* **2009**, *48*, 7752.

[13] a) K. Zhang, L. L. Zhang, X. S. Zhao, J. Wu, *Chem. Mater.* **2010**, *22*, 1392; b) J. Yan, T. Wei, B. Shao, Z. Fan, W. Qian, M. Zhang, F. Wei, *Carbon* **2010**, *48*, 487; c) Y. Zhao, H. Bai, Y. Hu, Y. Li, L. Qu, S. Zhang, G. Shi, *J. Mater. Chem.* **2011**, *21*, 13978; d) J. Yan, T. Wei, Z. Fan, W. Qian, M. Zhang, X. Shen, F. Wei, *J. Power Sources* **2010**, *195*, 3041; e) J. Jang, J. Bae, M. Choi, S. H. Yoon, *Carbon* **2005**, *43*, 2730; f) J. Xu, K. Wang, S.-Z. Zu, B.-H. Han, Z. Wei, *ACS Nano* **2010**, *4*, 5019.

[14] U. J. Lee, S.-H. Lee, J. J. Yoon, S. J. Oh, S. H. Lee, J. K. Lee, *Sol. Energy Mater. Sol. Cells* **2013**, *108*, 50.

[15] J. Zhang, J. Jiang, H. Li, X. S. Zhao, *Energy Environ. Sci.* **2011**, *4*, 4009.

[16] Z.-S. Wu, W. Ren, L. Gao, J. Zhao, Z. Chen, B. Liu, D. Tang, B. Yu, C. Jiang, H.-M. Cheng, *ACS Nano* **2009**, *3*, 411.

[17] a) M.-I. Boyer, S. Quillard, E. Rebourt, G. Louarn, J. P. Buisson, A. Monkman, S. Lefrant, *J. Phys. Chem. B* **1998**, *102*, 7382; b) M. Jain, S. Annapoorni, *Synth. Met.* **2010**, *160*, 1727; c) J. E. Pereira da Silva, D. L. A. de Faria, S. I. Córdoba de Torresi, M. L. A. Temperini, *Macromolecules* **2000**, *33*, 3077; d) G. Louarn, M. Lapkowski, S. Quillard, A. Pron, J. P. Buisson, S. Lefrant, *J. Phys. Chem.* **1996**, *100*, 6998; e) G. Niaura, R. Mažeikienė, A. Malinauskas, *Synth. Met.* **2004**, *145*, 105.

[18] R. Mažeikienė, V. Tomkutė, Z. Kuodis, G. Niaura, A. Malinauskas, *Vib. Spectrosc.* **2007**, *44*, 201.

[19] a) S. Quillard, G. Louarn, S. Lefrant, A. Macdiarmid, *Phys. Rev. B* **1994**, *50*, 12496; b) A. Ray, G. E. Asturias, D. L. Kershner, A. F. Richter, A. G. MacDiarmid, A. J. Epstein, *Synth. Met.* **1989**, *29*, 141; c) K. L. Tan, E. T. Kang, K. G. Neoh, *Polym. Adv. Technol.* **1994**, *5*, 171; d) Z. Ping, *J. Chem. Soc., Faraday Trans.* **1996**, *92*, 3063.

[20] a) M. C. Bernard, A. Hugot-Le Goff, *Electrochim. Acta* **2006**, *52*, 595; b) S. Bhadra, N. K. Singha, D. Khastgir, *Polym. Int.* **2007**, *56*, 919.

[21] a) L. Dauginet-De Pra, S. Demoustier-Champagne, *Thin Solid Films* **2005**, *479*, 321; b) E. T. Kang, K. G. Neoh, K. L. Tan, *Prog. Polym. Sci.* **1998**, *23*, 277.

[22] a) A. Belmokhtar, A. Benyoucef, A. Zehhaf, A. Yahiaoui, C. Quijada, E. Morallon, *Synth. Met.* **2012**, *162*, 1864; b) A. Meneguzzi, M. C. Pham, J.-C. Lacroix, B. Piro, A. Adenier, C. A. Ferreira, P.-C. Lacaze, *J. Electrochem. Soc.* **2001**, *148*, B121.

[23] J. P. Pouget, M. E. Jozefowicz, A. J. Epstein, X. Tang, A. G. MacDiarmid, *Macromolecules* **1991**, *24*, 779.

[24] Z. Luo, X. Ma, D. Yang, L. Yuwen, X. Zhu, L. Weng, L. Wang, *Carbon* **2013**, *57*, 470.

[25] a) K. Lee, S. Cho, S. H. Park, A. J. Heeger, C. W. Lee, S. H. Lee, *Nature* **2006**, *441*, 65; b) H.-W. Park, T. Kim, J. Huh, M. Kang, J. E. Lee, H. Yoon, *ACS Nano* **2012**, *6*, 7624.

[26] a) M. D. Stoller, S. Park, Y. Zhu, J. An, R. S. Ruoff, *Nano Lett.* **2008**, *8*, 3498; b) H. Mi, X. Zhang, X. Ye, S. Yang, *J. Power Sources* **2008**, *176*, 403; c) B. C. Kim, J. S. Kwon, J. M. Ko, J. H. Park, C. O. Too, G. G. Wallace, *Synth. Met.* **2010**, *160*, 94.

[27] X.-M. Feng, R.-M. Li, Y.-W. Ma, R.-F. Chen, N.-E. Shi, Q.-L. Fan, W. Huang, *Adv. Funct. Mater.* **2011**, *21*, 2989.

[28] H. J. Park, J. Meyer, S. Roth, V. Skákalová, *Carbon* **2010**, *48*, 1088.

[29] L. Li, A.-R. O. Raji, H. Fei, Y. Yang, E. L. G. Samuel, J. M. Tour, *ACS Appl. Mater. Interfaces* **2013**, *5*, 6622.

[30] a) J. Cho, K.-H. Shin, J. Jang, *Synth. Met.* **2010**, *160*, 1119; b) H. Yoon, M. Chang, J. Jang, *Adv. Funct. Mater.* **2007**, *17*, 431.